

Adaptive evolution with aneuploidy and mutation

Ilia Kohanovski^{1,*}, Martin Pontz^{2,*}, Avihu H. Yona³, and Yoav Ram^{1,2,†}

¹School of Computer Science, Reichman University, Herzliya, Israel

²School of Zoology, Faculty of Life Sciences, Tel Aviv University, Tel Aviv, Israel

³Institute of Biochemistry, Food Science and Nutrition, Robert H. Smith Faculty of Agriculture, Food and Environment, The Hebrew University of Jerusalem, Israel

*These authors contributed equally to this work

†Corresponding author: yoav@yoavram.com

March 23, 2022

Abstract

Aneuploidy is common in eukaryotes, often leading to decreased cell growth and fitness. However, evidence from yeast and fungi, as well as human tumour cells, suggests that aneuploidy can be beneficial under stressful conditions and lead to elevated growth rates and adaptation. Importantly, aneuploidy differs from point mutations in rate, fitness effect, and reversibility. Here, we develop evolutionary models for adaptive evolution with both mutation and aneuploidy. These models are used within an approximate Bayesian computation framework to estimate the formation rate and fitness effect of aneuploidy and mutation from results of evolutionary experiments in which *Saccharomyces cerevisiae* adapted to heat stress: the experimental populations first acquired chromosome duplications, only to later revert back to a euploid state. We also analyze our models to estimate the effect of the aneuploidy and mutation rates on the expected adaptation time and the probability for adaptation via aneuploidy. Our results suggest that aneuploidy can be a transient adaptive solution, which can decelerate adaptation in a non-intuitive manner. By creating an evolutionary conflict between the individual and the population, aneuploidy further complicates the process of adaptation in cell populations.

Introduction

Aneuploidy is common in eukaryotes. Aneuploidy is an imbalance in the number of chromosomes in the cell: an incorrect karyotype. Evidence suggests aneuploidy is very common in eukaryotes, e.g. animals (Santaguida and Amon, 2015; Naylor and van Deursen, 2016; Bakhoun and Landau, 2017), and fungi (Pavelka et al., 2010; Zhu et al., 2016; Robbins et al., 2017; Todd et al., 2017). Aneuploidy has been implicated in cancer formation and progression (Boveri, 2008; Schwartzman et al., 2010): 90% of solid tumours and 50% of blood cancers are aneuploid (Santaguida and Amon, 2015). Aneuploidy is also linked to the emergence of drug resistance (Selmecki et al., 2009) and virulence (Möller et al., 2018) in fungal pathogens, which are under-studied (Rodrigues and Albuquerque, 2018) despite infecting close to a billion people per year, causing serious infections and significant morbidity in >150 million people per year and killing >1.5 million people per year (Selmecki et al., 2009; Rodrigues and Albuquerque, 2018). In addition, aneuploidy is common in protozoan pathogens of the *Leishmania* genus, a major global health concern (Mannaert et al., 2012).

Aneuploidy is generally deleterious. The molecular and genetic mechanisms involved in aneuploidy have been explored (Musacchio and Salmon, 2007; Sheltzer and Amon, 2011; Chen et al., 2012; Rancati and Pavelka, 2013; Gerstein et al., 2015; Shor and Perlin, 2015). Experiments with human and mouse embryos found that aneuploidy is usually lethal. It is also associated with developmental defects and lethality in other multicellular organisms (Sheltzer and Amon, 2011). For example, aneuploid mouse embryonic cells grow slower than euploid cells (Williams et al., 2008). Similarly, in unicellular eukaryotes growing in benign conditions, aneuploidy usually leads to slower growth and decreased overall fitness (Niwa et al., 2006; Torres et al., 2007; Pavelka et al., 2010; Sheltzer and Amon, 2011; Kasuga et al., 2016), in part due to proteotoxic stress caused by increased expression in aneuploid cells (Pavelka et al., 2010; Santaguida et al., 2015; Zhu et al., 2018) and hypo-osmotic-like stress (Tsai et al., 2019).

Aneuploidy can lead to adaptation. However, aneuploidy can be beneficial under stressful conditions due to the wide range of phenotypes it can produce, some of which are advantageous (Pavelka et al., 2010). Thus, aneuploidy can lead to rapid adaptation in unicellular eukaryotes (Gerstein et al., 2015; Torres et al., 2010; Hong and Gresham, 2014; Rancati et al., 2008), as well as to rapid growth of somatic tumour cells (Schwartzman et al., 2010; Sheltzer et al., 2017). For example, aneuploidy in *S. cerevisiae* facilitates adaptation to a variety of stressful conditions like heat and pH (Yona et al., 2012), copper (Covo et al., 2014; Gerstein et al., 2015), salt (Dhar et al., 2011), and nutrient limi-

tation (Dunham et al., 2002; Gresham et al., 2008). Importantly, aneuploidy can also lead to drug resistance in pathogenic fungi such as *Candida albicans* (Selmecki et al., 2008, 2010; Gerstein and Berman, 2018) and *Cryptococcus neoformans* (Sionov et al., 2010), which cause candidiasis and meningoencephalitis, respectively.

Transient adaptive solution. Aneuploidy differs from mutation due to its distinct properties. Chromosome duplication usually occurs more often than mutation and on average produces larger fitness effects. Yet, because it affects many genes on a whole chromosome or a chromosome fragment, aneuploidy also carries fitness costs. Thus, aneuploidy can be a *transient adaptive solution*: it can rapidly occur and fix in the population under stressful conditions, and can be rapidly lost when the cost outweighs the benefit—when stress is removed or after beneficial mutations occur. Experimental evidence of such a transient role of aneuploidy was demonstrated by Yona et al. (2012). They evolved populations of *S. cerevisiae* under strong heat or pH stress. The populations adapted to the heat and pH stress within 450 and 150 generations, and this adaptation was determined to be due to chromosome duplications. Much later, after more than 1500 and 750 generations, for the heat and pH stress, respectively, the populations reverted back to an euploid state, while remaining adapted to the stress and accumulating multiple mutations. However, under gradual heat stress, aneuploidy was not observed. Yona et al. (2012) concluded that aneuploidy serves as a transient adaptive solution, or a “quick fix”, which is expected to facilitate adaptation.

The present study. Here, we develop an evolutionary-genetic model that includes the effects of natural selection, genetic drift, aneuploidy, and mutation to examine the role of aneuploidy in adaptive evolution. This model follows a population of cells characterised by both their ploidy and their genotype. We fit this model to the experimental results of Yona et al. (2012) using an *approximate Bayesian computation* framework (Sisson et al., 2007) to infer model parameters, including selection coefficients and rates of aneuploidy and mutation, and to test hypotheses about the evolutionary process by performing model selection between different versions of the model. We also mathematically analyze this evolutionary-genetic model to estimate the effects of selection, mutation, and aneuploidy on the adaptation time and the probability for adaptation via aneuploidy.

Models and Methods

Evolutionary Models. We model the evolution of a population of cells using a Wright-Fisher model (Otto and Day, 2007), assuming a constant effective population size N , non-overlapping generations, and including the effects of natural selection, genetic drift, aneuploidy, and mutation. We focus on beneficial genetic modifications, neglecting the effects of deleterious and neutral mutations or karyotypic changes. The model allows for a single aneuploid karyotype (e.g., chromosome III duplication) and a single mutation to accumulate in the genotype. Thus, the model follows four genotypes (Figure 1): euploid wild-type, $2n$, the initial genotype; euploid mutant, $2n^*$, with the standard karyotype and a single beneficial mutation; aneuploid wild-type, $2n+1$, with an extra chromosome, i.e., following chromosome duplication; and aneuploid mutant, $2n+1^*$, with an extra chromosome and a beneficial mutation.

Transitions between the genotypes occur as follows (Figure 1A): Beneficial mutations from $2n$ to $2n^*$ and from $2n+1$ to $2n+1^*$ occur with probability μ , the mutation rate. We neglect back-mutations (i.e., from $2n^*$ to $2n$ and from $2n+1^*$ to $2n+1$). Aneuploidy is formed by chromosome mis-segregation, so that cells transition from $2n$ to $2n+1$ and from $2n+1^*$ to $2n^*$ with probability δ , the aneuploidy rate. That is, we assume chromosomes are gained and lost at the same rate, and we neglect events that form a less-fit genotype (i.e., $2n+1$ to $2n$ and $2n^*$ to $2n+1^*$). The fitness values of the four genotypes are given by Table 1.

The initial population has N cells with genotype $2n$. The effect of natural selection on the frequency f_i of genotype $i = 2n, 2n + 1, 2n + 1^*, \text{ or } 2n^*$ is given by

$$f_i^s = \frac{f_i w_i}{\bar{w}}, \quad (1)$$

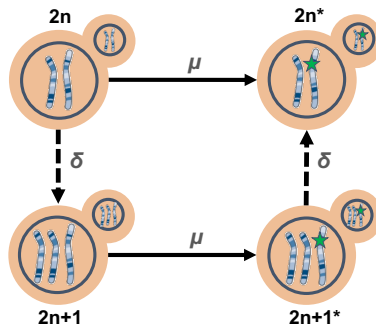


Figure 1: Model illustration. There are four genotypes in our model: euploid wild-type, $2n$; euploid mutant, $2n^*$; aneuploid wild-type, $2n+1$; and aneuploid mutant, $2n+1^*$. Overall there are two possible trajectories from $2n$ to $2n^*$. Arrows denote transitions between genotypes, with transition rates: μ , beneficial mutation rate; δ , aneuploidy rate.

Table 1: Fitness values.

| <i>Genotype i</i> | $2n$ | $2n+1$ | $2n+1^*$ | $2n^*$ |
|----------------------|------|-------------|----------------------|---------|
| <i>Fitness</i> w_i | 1 | $1 - c + b$ | $(1 - c)(1 + s) + b$ | $1 + s$ |

$s \geq 0$ is the selection coefficient of a beneficial mutation; $0 \leq c \leq 1$ is the fitness cost of aneuploidy; and $b \geq c$ is the selection coefficient, or fitness benefit, of aneuploidy.

where the fitness values w_i are given in Table 1 and $\bar{w} = \sum_j f_j w_j$ is the population mean fitness. The effect of mutation and aneuploidy on genotype frequencies is given by

$$\begin{aligned} f_{2n}^m &= (1 - \delta - \mu)f_{2n}^s, \\ f_{2n+1}^m &= \delta f_{2n}^s + (1 - \mu)f_{2n+1}^s, \\ f_{2n+1^*}^m &= \mu f_{2n+1}^s + (1 - \delta)f_{2n+1^*}^s, \\ f_{2n^*}^m &= \mu f_{2n}^s + \delta f_{2n+1}^s + f_{2n^*}^s. \end{aligned} \tag{2}$$

Finally, random genetic drift is modeled using a multinomial distribution (Otto and Day, 2007),

$$\mathbf{f}' \sim \frac{1}{N} \cdot \text{Mult}(N, \mathbf{f}^m), \tag{3}$$

where $\mathbf{f}^m = (f_{2n}^m, f_{2n+1}^m, f_{2n+1^*}^m, f_{2n^*}^m)$ are the frequencies of the genotypes after mutation and aneuploidy, \mathbf{f}' are the genotype frequencies in the next generation, and $\text{Mult}(N, \mathbf{f})$ is a multinomial distribution parameterized by the population size N and the genotype frequencies \mathbf{f} . Overall, the change in genotype frequencies from one generation to the next is given by the transformation $f_i \rightarrow f'_i$.

Empirical evidence. We use the results of evolutionary experiments reported by Yona et al. (2012). In their heat-stress experiment, four populations of *S. cerevisiae* evolved under 39 °C. Aneuploidy fixed in all four population in the first 450 generations (hereafter, fixation or elimination of a genotype by *generation t* means that more than 95% or less than 5% of the population carry the genotype at generation t , and possibly earlier). From unpublished results, aneuploidy did not fix before at least 200 generations elapsed. The experiment continued with two populations, in which aneuploidy was eliminated by generation 1,700 and 2,350.

Likelihood function. Because our model, just like the Wright-Fisher model, is non-linear and stochastic, computing the distribution of fixation time $T(g)$ of genotype g for use in the likelihood function is intractable (it is even hard to use a diffusion-equation approximation due to the model having multiple genotypes, rather than just two). We overcome this problem by approximating the likelihood

using simulations. We simulate 1,000 experiments per parameter vector $\theta = (\mu, \delta, s, b, c)$, resulting in a set of simulated observations $\tilde{\mathbf{X}} = \{\tilde{X}_i\}_{i=1}^{1000}$. We then compute the approximate likelihood,

$$\begin{aligned}\mathcal{L}(\theta) = P^4(200 \leq T(2n+1) \leq 450) \cdot & \left[1 - \right. \\ & P_{\tilde{\mathbf{X}}}^4(\{T(2n^*) < 1700\} \mid 200 \leq T(2n+1) \leq 450) - \\ & P_{\tilde{\mathbf{X}}}^4(\{1700 < T(2n^*) < 2350\} \mid 200 \leq T(2n+1) \leq 450) + \\ & \left. P_{\tilde{\mathbf{X}}}^4(\{T(2n^*) < 1700\} \wedge \{1700 < T(2n^*) < 2350\} \mid 200 \leq T(2n+1) \leq 450) \right],\end{aligned}\tag{4}$$

where $!\{\dots\}$ is the "logical not" operator, $P^4(\dots)$ is the 4th power of $P(\dots)$, and all probabilities $P_{\tilde{\mathbf{X}}}(\dots)$ are approximated from the results of the simulations $\tilde{\mathbf{X}}$. For example, $P_{\tilde{\mathbf{X}}}(\{T(2n^*) < 1700\} \mid 200 \leq T(2n+1) \leq 450)$ is approximated by taking simulations in which $2n+1$ fixed before generation 450 but not before generation 200, and computing the fraction of such simulations in which $2n^*$ did not fix by generation 1,700, and hence aneuploidy did not extinct before generation 1,700. Figure S4 compares results with less and more simulated experiments, demonstrating that 1,000 simulations are likely enough.

For a model without aneuploidy (that is, when the aneuploidy rate is fixed at zero, $\delta = 0$), we disregard the increased expression in chromosome III and the growth advantage measured in generation 450, and focus on the growth advantage measured in later generations, presumably due to a beneficial mutation. Therefore, the likelihood is approximated by

$$\begin{aligned}\mathcal{L}_!(\theta) = 1 - & P_{\tilde{\mathbf{X}}}^4(\{T(2n^*) < 1700\}) - \\ & P_{\tilde{\mathbf{X}}}^4(\{1700 < T(2n^*) < 2350\}) + \\ & P_{\tilde{\mathbf{X}}}^4(\{T(2n^*) < 1700\} \wedge \{1700 < T(2n^*) < 2350\}).\end{aligned}\tag{5}$$

Parameter inference. To infer model parameters, we use approximate Bayesian computation with a sequential Monte-Carlo scheme, or ABC-SMC (Sisson et al., 2007), implemented in the `pyABC` Python package (Klinger et al., 2018, pyabc.readthedocs.io). This approach uses numerical stochastic simulations of the model to infer a posterior distribution over the model parameters. It is a method of likelihood-free, simulation-based inference (Cranmer et al., 2020), that is, for estimating a posterior distribution when a likelihood function cannot be directly computed. It is therefore suitable in our case, in which the likelihood function can only be approximated from simulations, and cannot be directly computed.

The ABC-SMC algorithm employs sequential importance sampling over multiple iterations (Toni et al., 2009; Klinger and Hasenauer, 2017; Syga et al., 2021). In iteration t of the algorithm, a

set of parameter vectors, $\{\theta_{i,t}\}_{i=1}^{n_t}$, also called *particles*, are constructed in the following way. A proposal particle, θ^* , is sampled from a proposal distribution, and is either accepted or rejected, until n_t particles are accepted. The number of particles, n_t , is adapted at every iteration t using the adaptive population strategy (Klinger et al., 2018, pyabc.readthedocs.io). For $t = 0$, the proposal particle is sampled from the prior distribution, $p(\theta)$. For $t > 0$, the proposal particle is sampled from the particles accepted in the previous iteration, $\{\theta_{i,t-1}\}_{i=1}^{n_{t-1}}$, each with a probability relative to its weight $W_{t-1}(\theta_{i,t-1})$ (see below). The proposal particle is then perturbed using a kernel perturbation kernel, $K_t(\theta^* | \theta)$ where θ is the sample from the previous iteration. Then, a set of synthetic observations $\tilde{\mathbf{X}}^*$ is simulated, and the proposal particle θ^* is accepted if its approximate likelihood (Equation (4)) is high enough, $\mathcal{L}(\theta^*) > 1 - \epsilon_t$ (or more commonly, if $1 - \mathcal{L}(\theta^*) < \epsilon_t$), where $\epsilon_t > 0$ is the *acceptance threshold*, as higher values of ϵ_t allow more particles to be accepted. The acceptance threshold ϵ_t is chosen as the median of the $1 - \mathcal{L}(\theta)$ of the particles accepted in the previous iteration, $t - 1$, and $\epsilon_0 = 0.01$. For each accepted particle $\theta_{i,t}$ a weight $W_t(\theta_{i,t})$ is assigned: for $t = 0$, $W_0(\theta_{i,0}) = 1$, and for $t > 0$, $W_t(\theta_{i,t}) = p(\theta_{i,t}) / \sum_{i=1}^{n_{t-1}} W_{t-1}(\theta_{i,t-1}) K_t(\theta_{i,t}, \theta_{i,t-1})$, where $p(\theta)$ is the prior density of θ and $K_t(\theta', \theta)$ is the probability of a perturbation from θ to θ' . $K_t(\theta' | \theta)$ is a multivariate normal distribution, fitted at iteration t to the particles from the previous iteration, $\{\theta_{i,t-1}\}_{i=1}^{n_{t-1}}$, and their weights, $\{W(\theta_{i,t-1})\}_{i=1}^{n_{t-1}}$.

Acceptance is determined according to the approximate likelihood (Equation (4)), which has a maximum value of 0.875. Thus, we terminated the inference when $\epsilon \leq 0.13$ after six iterations, with $n_6 = 982$ accepted parameter vectors and effective sample size ESS=651 (Figure S3). Running the inference algorithm with different initialization seeds and less or more simulations for approximating the likelihood produced similar posterior distributions (Figure S4).

After producing a set of weighted particles from the the posterior distribution using the above ABC-SMC algorithm, we approximate the posterior using kernel density estimation (KDE) with Gaussian kernels, from which we find the MAP (maximum a posteriori) estimate as the maximum of the KDE function. We then draw 50,000 samples from the posterior KDE to compute the HDI (highest density interval) and visualize the posterior distribution with histograms.

Model comparison. The main criterion that we use for model selection is WAIC, the widely applicable information criterion (Gelman et al., 2013),

$$WAIC(\theta) = -2 \log \mathbb{E}[\mathcal{L}(\theta)] + 2\mathbb{V}[\log \mathcal{L}(\theta)] \quad (6)$$

where θ is a parameter vector, and $\mathbb{E}[\cdot]$ and $\mathbb{V}[\cdot]$ are the expectation and variance taken over the posterior distribution, which in practice are approximated using 50,000 samples from the posterior KDE. WAIC values are scaled as a deviance measure: lower values imply higher predictive accuracy (Kass and Raftery, 1995).

We also plot posterior predictions: for each model we execute 10,000 simulations using the MAP parameter estimates and plot the distributions of time to fixation of $2n^*$, one of key properties of the model likelihood. These plots visualize the fit of each model to the data. Also, for similar models we plot the marginal and joint posterior distributions of the parameters; if these are similar, we consider the models are interchangeable. We validate this by comparing HDI (highest density interval) of posterior distributions.

Prior distributions. We used informative prior distributions for $w_{2n+1} = 1 - c + b$, $w_{2n+1^*} = (1 + s)(1 - c) + b$ and $w_{2n^*} = 1 + s$, which we estimated from growth curves data from mono-culture growth experiments previously reported by Yona et al. (2012, Figs. 3C, 4A, and S2). We used **Curveball**, a method for predicting results of competition experiments from growth curve data (Ram et al., 2019, curveball.yoavram.com). Briefly, **Curveball** takes growth curves of two strains growing separately in mono-culture and predicts how they would grow in a mixed culture, that is, it predicts the results of a competition assay. From these predictions, relative fitness values can be computed. Because **Curveball** uses a maximum-likelihood approach to estimate model parameters, we were able to estimate a distribution of relative fitness values by sampling from a truncated multivariate normal distribution defined by the maximum-likelihood covariance matrix.

We sampled 10,000 samples to use as a prior distribution (Figure S1). We used growth curves of $2n$ and $2n+1$ in 39 °C to estimate a prior distribution for w_{2n+1} (Figure S1-D, assuming $w_{2n} = 1$). In lieu of a more suitable prior, we used the same prior for w_{2n+1^*} and w_{2n^*} . To increase computational efficiency, we also assumed $w(2n^*) > w(2n+1^*) > w(2n+1) > w(2n)$; running the inference without this assumption produced similar results. We also examined an extended informative prior that uses additional growth curves of $2n^*$ (*refined* strain from Yona et al. (2012)) and $2n+1$ in 39 °C to estimate w_{2n^*}/w_{2n+1} (Figure S1L). The same prior was used for w_{2n^*}/w_{2n+1^*} .

As a control, we tested an uninformative uniform prior with $U(1, 6)$, for (i) all w_{2n+1} , w_{2n+1^*} , w_{2n^*} , or (ii) only for w_{2n+1^*} , w_{2n^*} , using the above informative prior for w_{2n+1} . In these cases the inference algorithm failed to converge.

For the mutation rate, μ , and aneuploidy rate, δ , we used uninformative uniform priors, $\mu \sim$

$U(10^{-9}, 10^{-5})$ and $\delta \sim U(10^{-6}, 10^{-2})$. A wider mutation rate prior, $\mu \sim U(10^{-9}, 10^{-3})$, produced similar results.

Results

Statistical inference

Parameter estimation. We used ABC-SMC to infer the posterior distribution of model parameters (Figure 2). We report parameter estimates using the MAP (maximum a posteriori) and providing the 50% HDI (highest density interval) in square brackets. The estimated aneuploidy rate, $\delta = 1.722 \cdot 10^{-3}$ [$1.394 \cdot 10^{-3} - 2.754 \cdot 10^{-3}$], agrees with previous estimates. The estimated mutation rate, $\mu = 2.942 \cdot 10^{-6}$ [$2.017 \cdot 10^{-7} - 4.15 \cdot 10^{-6}$], corresponds to a mutation target size of 10^4 , assuming the mutation rate per base pair is roughly $2 \cdot 10^{-10}$ (Zhu et al., 2014) or $3.3 \cdot 10^{-10}$ (Lynch et al., 2008). The estimated fitness values are $w_{2n+1} = 1.022$ [$1.021 - 1.023$], $w_{2n+1*} = 1.025$ [$1.024 - 1.026$], $w_{2n*} = 1.028$ [$1.026 - 1.029$], all relative to the fitness of $2n$, which is set to $w_{2n} = 1$. Thus, we can infer that the benefit and cost of trisomy was $b = 2.5\%$ and $c = 0.3\%$, and the benefit of the beneficial mutation was 2.8% (Table 1).

Model checking and comparison. The model fits the data well: in simulations using the MAP parameter estimates, $2n^*$ fixed in 61% of simulations by generation 1,700 and in 100% of simulations by generation 2,350 (Figure 4B). Interestingly, the genotype frequency dynamics in these simulations demonstrate that $2n+1^*$ never reaches substantial frequency (Figure 5).

Moreover, a model without aneuploidy (where the aneuploidy rate is fixed at zero, $\delta = 0$), fails to explain the experimental observations (Figure 4). The estimated mutation rate without aneuploidy is $\mu = 7.979 \cdot 10^{-9}$ [$7.903 \cdot 10^{-9} - 8.135 \cdot 10^{-9}$], much lower compared to a model with aneuploidy and suggesting a target size of just 40. The fitness of the mutant is also much lower at $w_{2n*} = 1.013$ [$1.012 - 1.013$]. This is because, without aneuploidy, a high mutation rate or fitness effect will lead to faster appearance and fixation of $2n^*$ than in the experimental observations. Even with these lower estimates, the model fit is worse than that of a model with aneuploidy (Figure 4).

We also inferred model parameters under the assumption that the mutation rate increases in aneuploid cells by a factor $\tau = 33/32$ (due to an additional chromosome), 2, 5, 10, or 100 (due to genetic instability). We found that the posterior distribution was similar for $\tau = 1, 33/32, 2$, and 5 (Figure S5). With $\tau = 100$, the estimated mutation rate was about 7-8-fold lower compared to $\tau = 1$ ($\mu =$

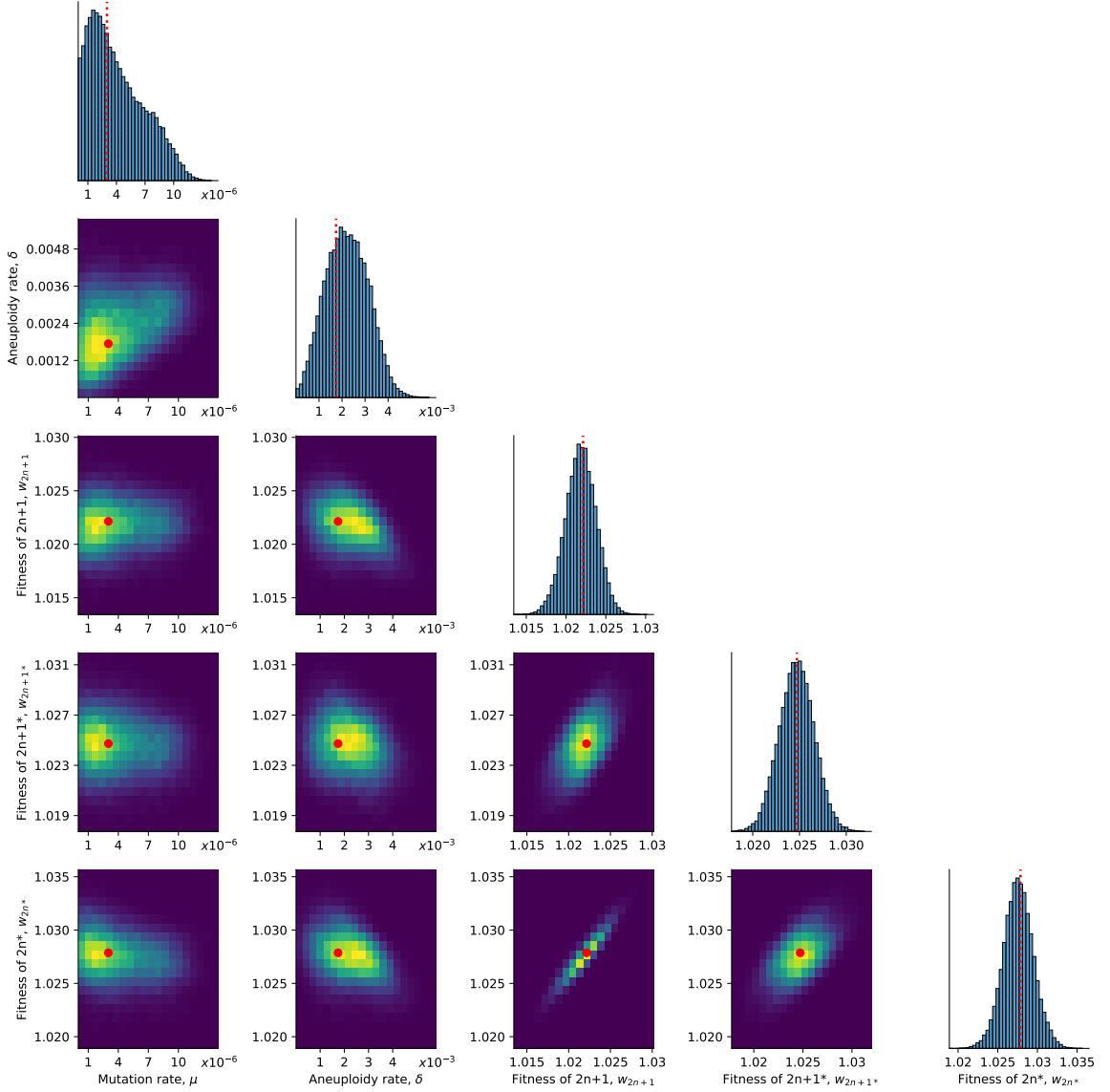


Figure 2: Posterior distribution of model parameters. On the diagonal, the inferred posterior distribution of each model parameter. Below the diagonal, the inferred joint posterior distribution of pairs of model parameters (dark purple and bright yellow for low and high density, respectively). Red markers and orange lines for the joint MAP estimate (which may differ from the marginal MAP, as the marginal distribution integrates over all other parameters).

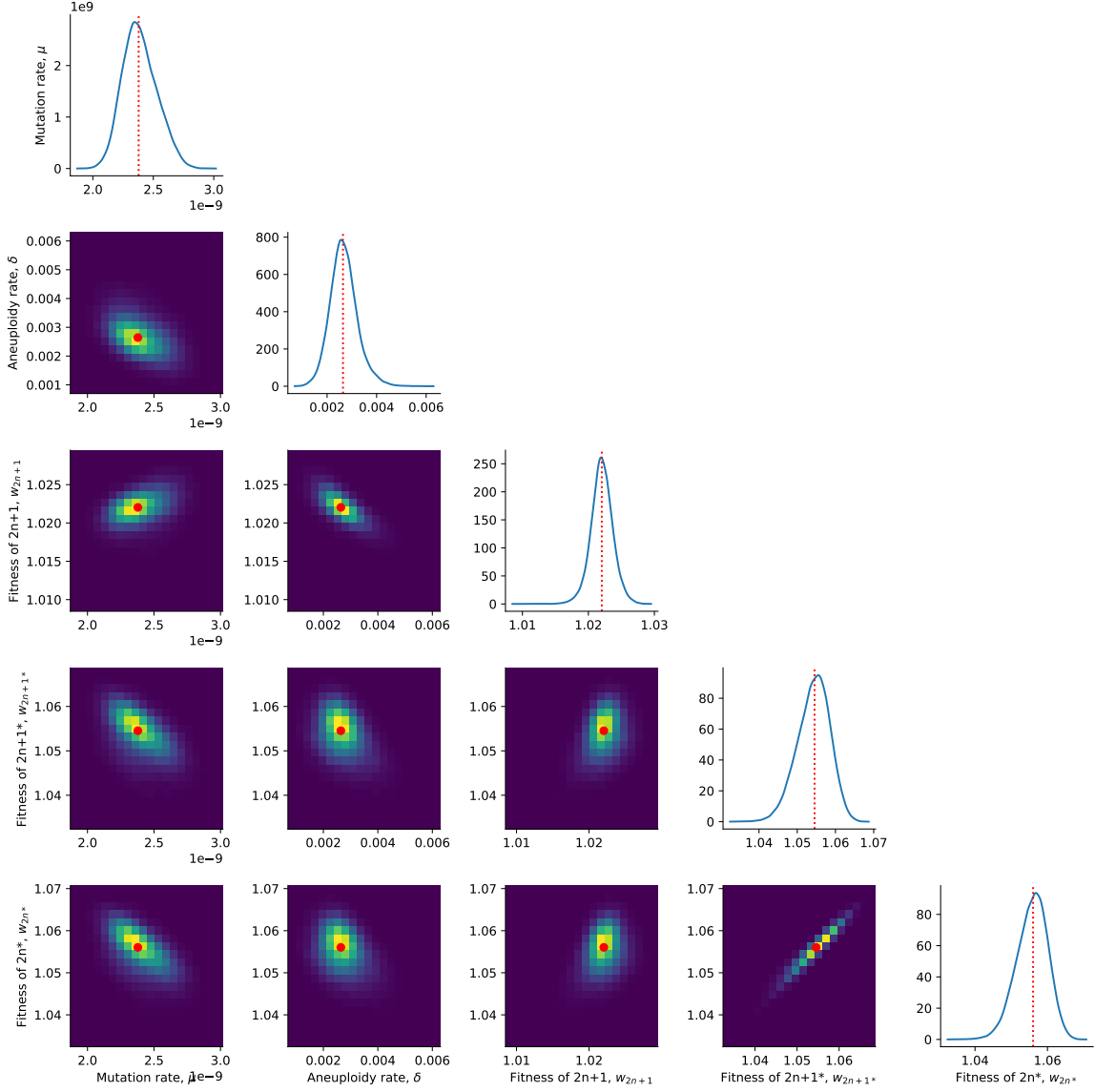


Figure 3: Posterior distribution of parameters inferred with the extended prior distribution. On the diagonal, the inferred posterior distribution of each model parameter. Below the diagonal, the inferred joint posterior distribution of pairs of model parameters (dark purple and bright yellow for low and high density, respectively). Red markers and orange lines for the joint MAP estimate (which may differ from the marginal MAP, as the marginal distribution integrates over all other parameters).

$3.81 \cdot 10^{-7}$ [$1.508 \cdot 10^{-7} - 4.995 \cdot 10^{-7}$]) and the aneuploidy rate was about 2-3-fold lower ($\delta = 0.782 \cdot 10^{-3}$ [$0.661 \cdot 10^{-3} - 1.462 \cdot 10^{-3}$]). With $\tau = 10$, the estimated mutation rate was only slightly lower compared to $\tau = 1$ ($\mu = 1.674 \cdot 10^{-6}$ [$2.501 \cdot 10^{-7} - 1.741 \cdot 10^{-6}$]). WAIC is lowest for $\tau = 100$ (Table S1), and if we rule such a strong effect of genetic instability a-priori, the next two lowest WAIC values are for $\tau = 33/32$ and $\tau = 5$. Therefore, we cannot rule out an increased mutation rate in aneuploid cells, but unless the effect is strong ($\tau = 100$), it does not seem to affect our inference results. We also checked the differences in fixation/loss times of $2n$, $2n+1$ and $2n^*$ for the models with different τ . We saw that the models can be distinguished using these parameters, especially $\tau = 100$ (Figure 6).

Sensitivity analysis shows that changing a single parameter while keeping the rest fixed at the MAP estimate produces a worse fit to the data (Figure S2). Furthermore, we fitted models with a mutation rate fixed at $\mu=10^{-5}$, 10^{-6} and 10^{-7} . We inferred similar parameters estimates for the model with $\mu = 10^{-6}$ compared to the model with a free μ parameter. Models with $\mu=10^{-5}$ and $\mu=10^{-7}$ inferred different parameters estimates (Figure S6). WAIC was lower when μ is fixed (Table S1), but this is not surprising, as WAIC attempt to balance between model fit and model complexity, where the latter takes into account the number of model parameters.

Finally, we estimated the parameters under an extended informative prior (see *Prior distributions*), with different priors for w_{2n+1*} and w_{2n*} . The estimated mutation rate was much lower compared to the basic prior, with $\mu = 2.379 \cdot 10^{-9}$ [$2.267 \cdot 10^{-9} - 2.458 \cdot 10^{-9}$]. Other parameter estimates are: $\delta = 2.636 \cdot 10^{-3}$ [$2.245 \cdot 10^{-3} - 2.919 \cdot 10^{-3}$], $w_{2n+1} = 1.022$ [$1.021 - 1.023$], $w_{2n+1*} = 1.032$ [$1.03 - 1.035$], $w_{2n*} = 1.033$ [$1.031 - 1.036$]. The WAIC of the model is much lower: -57 compared to 295 (Table S1).

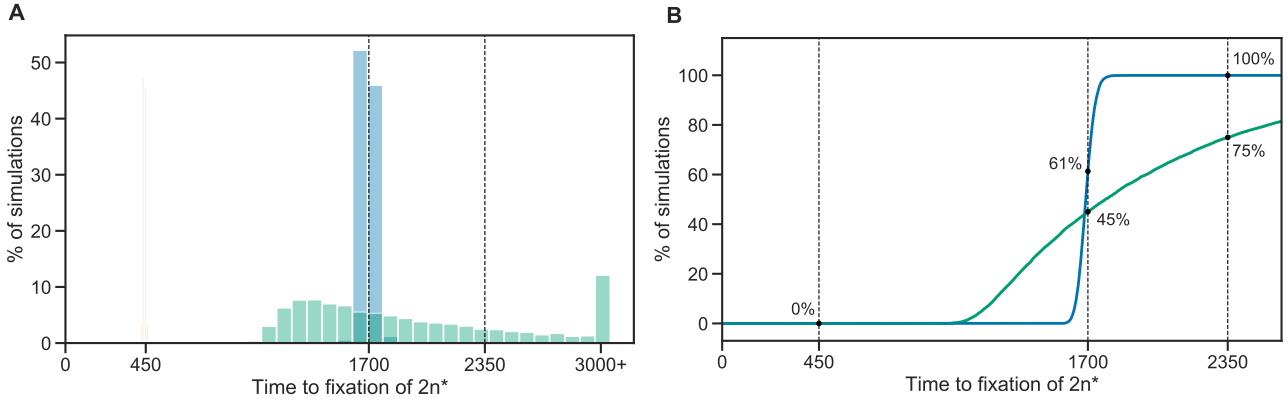


Figure 4: Model fit with and without aneuploidy. (A) The distribution of time to fixation of $2n^*$ (i.e., adaptation time) in 10,000 simulations of the model with aneuploidy (blue; MAP parameters) compared to two models without aneuploidy: a model with the same parameter values except $\delta = 0$ (orange), and a model fitted to the data assuming $\delta = 0$ (green). In the experiment by Yona et al. (2012), one population lost aneuploidy by generation 1,700 and another by generation 2,350 (dashed lines) but not before generation 450. Thus, the blue distribution is a better fit compared to the green, and the yellow histogram has a very poor fit. The last bin contains all the simulations with time equal or greater than 3,000. (B) Cumulative distribution of the time to fixation of $2n^*$ in 10,000 simulations using the MAP estimate with and without aneuploidy in blue and green, respectively, and corresponding to the blue and green bars in panel A. The MAP likelihood (Equation (4)) is 0.84 and 0.67 with and without aneuploidy, respectively.

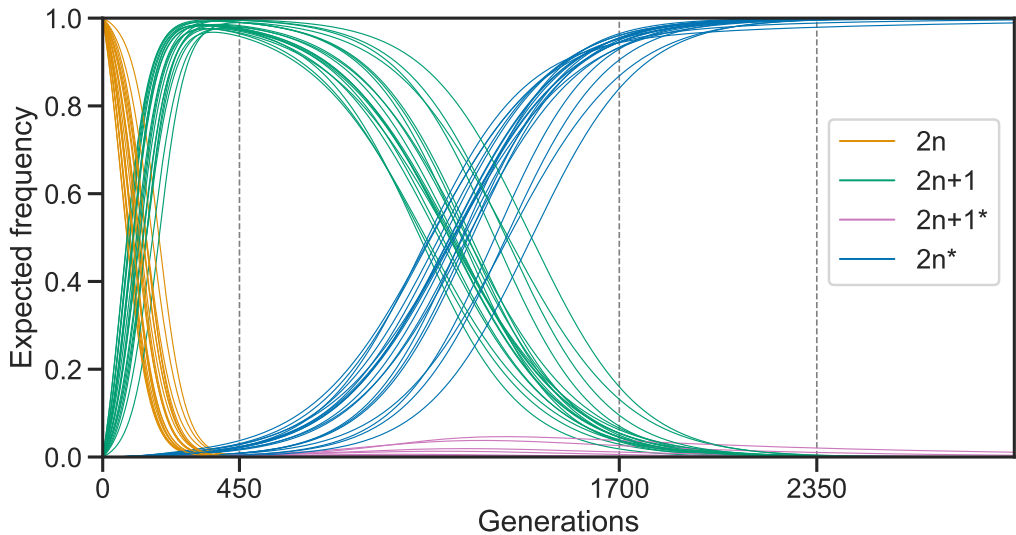


Figure 5: Posterior genotype frequency dynamics for the model. The posterior prediction for the frequencies of the four genotypes over time. Each of the 20 curves is the average of 10,000 simulations of the model using parameters drawn from the posterior distribution.

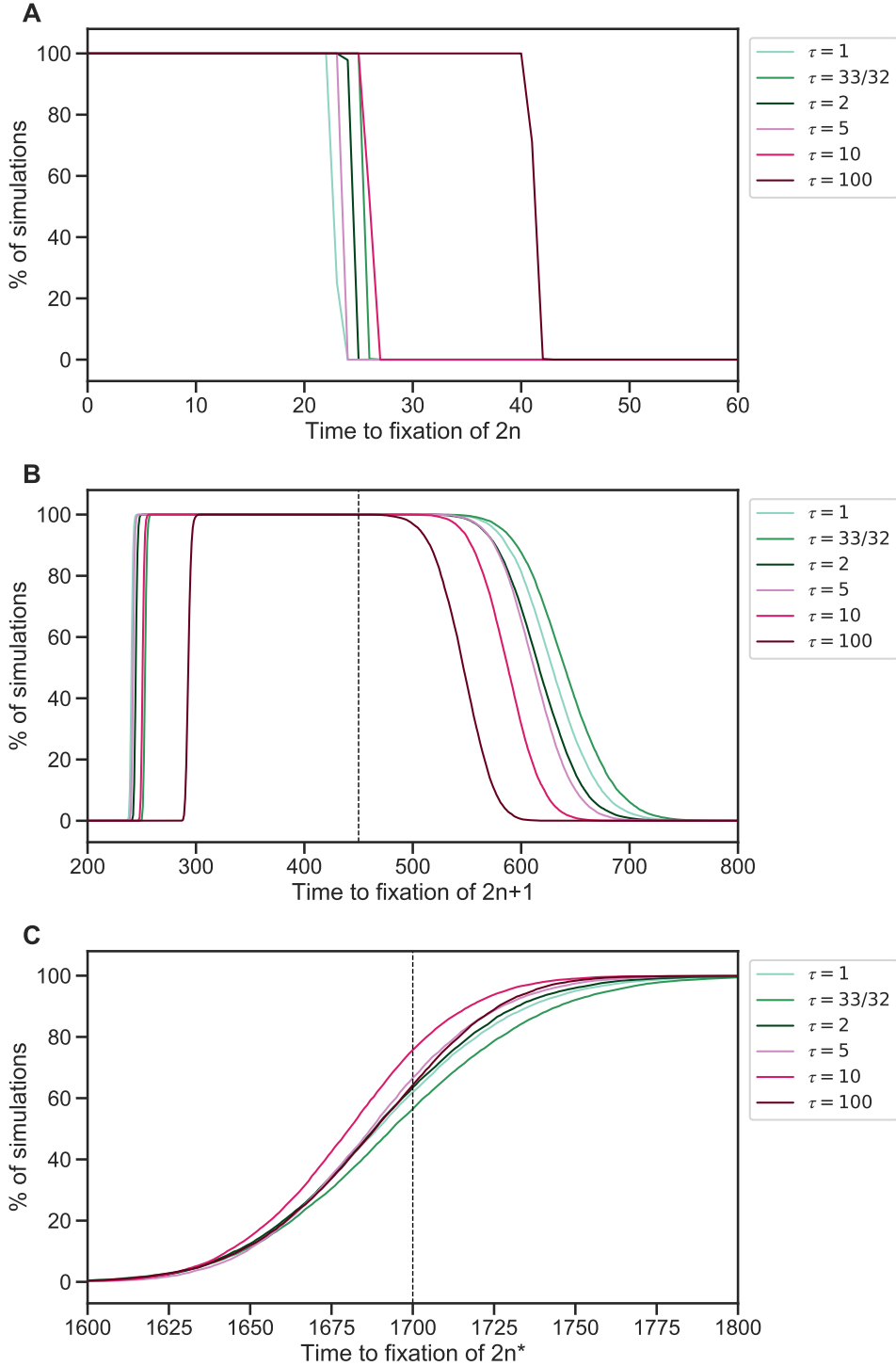


Figure 6: Genotype fixations for models with different τ . We estimated the parameters for different models, each assuming a different value of τ , the fold-increase in mutation rate in aneuploid cells. We then generated 10,000 simulations using the MAP estimate of each model and evaluated the fraction of simulations in which the genotype $2n$ (A), $2n+1$ (B), and $2n^*$ (C) is fixed (y-axis) at each generation (x-axis). Note that $2n+1^*$ did not fix. We can see that $\tau = 100$ can be distinguished if time to loss of $2n$ is known (panel A) or if time to fixation or loss of $2n+1$ is known (panel B). It is harder to distinguish between $1 \leq \tau \leq 10$.

Analysis

Discussion

Aneuploidy is not just another type of mutation. The published data indicate that, like mutation, aneuploidy can be both deleterious and beneficial (Pavelka et al., 2010; Sheltzer and Amon, 2011). Nevertheless, there are important and fundamental differences between adaptation by aneuploidy and adaptation by beneficial mutations (Yona et al., 2015), which make aneuploidy a unique mechanism for generating genetic variation. First, the aneuploidy rate (i.e. the frequency of mis-segregation events) is significantly higher than the mutation rate (Santaguida and Amon, 2015). Thus, everything else being equal, adaptation by aneuploidy will be faster and more frequent. Second, fitness effects of aneuploidy are larger than those of the majority of mutations, on average, and are rarely neutral (Pavelka et al., 2010; Yona et al., 2012; Sunshine et al., 2015), allowing selection to quickly sort deleterious and beneficial genotypes. Third, the number of different karyotypes is considerably smaller than the number of different genotypes, and different karyotypes are likely to have different phenotypes (Pavelka et al., 2010). Therefore, exploration of the phenotype space by aneuploidy requires smaller populations and a shorter time span. Fourth, aneuploidy is a reversible state, as the rate of chromosome loss is high and the cost of aneuploidy is significant (Niwa et al., 2006). Indeed, aneuploidy often provides a transient solution: under short-term stress conditions, aneuploidy reverts (chromosome number returns to normal) when the stress subsides; under long-term stress conditions, aneuploidy reverts when refined solutions, generated by beneficial mutations, take over (Yona et al., 2012). Finally, aneuploidy results in increased genome instability, potentially increasing genetic variation by a positive feedback loop (Rancati and Pavelka, 2013; Bouchonville et al., 2009; Zhu et al., 2012), while also increasing its own transience.

Evolutionary theory of aneuploidy. The role of aneuploidy in adaptation has only recently been observed (Sionov et al., 2010; Yona et al., 2012; Gerstein et al., 2015), and is largely missing from the literature on evolution and adaptation: the introductory textbook *Evolution* by Bergstrom and Dugatkin (2012) does not mention the word aneuploidy, and the graduate-level book *Mutation-Driven Evolution* by Nei (2013) only briefly mentions aneuploidy in the context of speciation, but not adaptation. In recent reviews of the literature, aneuploidy is suggested to play an important role in fungal adaptation (Robbins et al., 2017; Todd et al., 2017) and cancer evolution (Santaguida and Amon, 2015; Naylor and van Deursen, 2016; Sansregret and Swanton, 2017), yet these reviews cite no theoretical studies nor any quantitative models. Indeed, evolutionary, ecological, and epidemiological studies

mostly assume adaptation occurs via beneficial mutations, recombination, and sex. Therefore, there is a critical need to develop an evolutionary theory of aneuploidy like the evolutionary theories of other mechanisms for generation of genetic variation, e.g. mutation (Lynch, 2010), recombination (Hartfield and Keightley, 2012), and sex (Otto, 2009). An evolutionary theory of aneuploidy will be central to the interpretation of experimental and clinical observations and design of new hypotheses, experiments, and treatments (Carja et al., 2014). For example, despite the lack of theoretical models, aneuploidy has been invoked in a new strategy to combat pathogens and tumour cells by setting “evolutionary traps” (Gerstein et al., 2015; Chen et al., 2015), in which a condition that predictably leads to emergence of aneuploidy is applied, followed by a condition that specifically selects against aneuploid cells.

Acknowledgements

We thank Yitzhak Pilpel, Orna Dahan, Lilach Hadany, Judith Berman, David Gresham, Shay Covo, Martin Kupiec, and Tal Simon for discussions and comments. This work was supported in part by the Israel Science Foundation (YR 552/19) and Minerva Stiftung Center for Lab Evolution (YR).

References

- Bakhoum, S. F. and Landau, D. A. (2017), ‘Chromosomal instability as a driver of tumor heterogeneity and evolution’, *Cold Spring Harb. Perspect. Med.* **7**(6), 1–14.
- Bergstrom, C. T. and Dugatkin, L. A. (2012), *Evolution*, 1 edn, W. W. Norton & Company, New York, NY.
- Bouchonville, K., Forche, A., Tang, K. E. S., Semple, C. a. M. and Berman, J. (2009), ‘Aneuploid chromosomes are highly unstable during DNA transformation of *Candida albicans*.’, *Eukaryot. Cell* **8**(10), 1554–66.
- Boveri, T. (2008), ‘Concerning the Origin of Malignant Tumours’, *J. Cell Sci.* **121**(Supplement 1), 1–84.
- Carja, O., Liberman, U. and Feldman, M. W. (2014), ‘Evolution in changing environments: Modifiers of mutation, recombination, and migration’, *Proc. Natl. Acad. Sci.* p. 201417664.
- Chen, G., Mulla, W. A., Kucharavy, A., Tsai, H.-J., Rubinstein, B., Conkright, J., McCroskey, S., Bradford, W. D., Weems, L., Haug, J. S., Seidel, C. W., Berman, J. and Li, R. (2015), ‘Targeting the Adaptability of Heterogeneous Aneuploids’, *Cell* **160**(4), 771–784.
- Chen, G., Rubinstein, B. and Li, R. (2012), ‘Whole chromosome aneuploidy: Big mutations drive adaptation by phenotypic leap’, *BioEssays* **34**(10), 893–900.
- Covo, S., Puccia, C. M., Argueso, J. L., Gordenin, D. A. and Resnick, M. A. (2014), ‘The sister chromatid cohesion pathway suppresses multiple chromosome gain and chromosome amplification.’, *Genetics* **196**(2), 373–384.
- Cranmer, K., Brehmer, J. and Louppe, G. (2020), ‘The frontier of simulation-based inference’, *Proc. Natl. Acad. Sci. U. S. A.* p. 201912789.
- Dhar, R., Sägesser, R., Weikert, C., Yuan, J. and Wagner, A. (2011), ‘Adaptation of *Saccharomyces cerevisiae* to saline stress through laboratory evolution.’, *J. Evol. Biol.* **24**(5), 1135–53.

- Dunham, M. J., Badrane, H., Ferea, T., Adams, J., Brown, P. O., Rosenzweig, F. and Botstein, D. (2002), ‘Characteristic genome rearrangements in experimental evolution of *Saccharomyces cerevisiae*’, *Proc. Natl. Acad. Sci.* **99**(25), 16144–16149.
- Gelman, A., Carlin, J. B., Stern, H. S., Dunson, D. B., Vehtari, A. and Rubin, D. B. (2013), *Bayesian Data Analysis, Third Edition*, Chapman & Hall/CRC Texts in Statistical Science, Taylor & Francis.
- Gerstein, A. C. and Berman, J. (2018), ‘Diversity of acquired adaptation to fluconazole is influenced by genetic background and ancestral fitness in *Candida albicans*’, *bioRxiv* p. 360347.
- Gerstein, A. C., Ono, J., Lo, D. S., Campbell, M. L., Kuzmin, A. and Otto, S. P. (2015), ‘Too much of a good thing: the unique and repeated paths toward copper adaptation.’, *Genetics* **199**(2), 555–71.
- Gresham, D., Desai, M. M., Tucker, C. M., Jenq, H. T., Pai, D. A., Ward, A., DeSevo, C. G., Botstein, D. and Dunham, M. J. (2008), ‘The repertoire and dynamics of evolutionary adaptations to controlled nutrient-limited environments in yeast’, *PLoS Genet.* **4**(12).
- Hartfield, M. and Keightley, P. D. (2012), ‘Current hypotheses for the evolution of sex and recombination.’, *Integr. Zool.* **7**(2), 192–209.
- Hong, J. and Gresham, D. (2014), ‘Molecular Specificity, Convergence and Constraint Shape Adaptive Evolution in Nutrient-Poor Environments’, *PLoS Genet.* **10**(1).
- Kass, R. E. and Raftery, A. E. (1995), ‘Bayes Factors’, *J. Am. Stat. Assoc.* **90**(430), 773.
- Kasuga, T., Bui, M., Bernhardt, E., Swiecki, T., Aram, K., Cano, L. M., Webber, J., Brasier, C., Press, C., Grünwald, N. J., Rizzo, D. M. and Garbelotto, M. (2016), ‘Host-induced aneuploidy and phenotypic diversification in the Sudden Oak Death pathogen *Phytophthora ramorum*’, *BMC Genomics* **17**(1), 1–17.
- Kimura, M. and Ohta, T. (1969), ‘The Average Number of Generations until Fixation of a Mutant Gene in a Finite Population.’, *Genetics* **61**(3), 763–71.
- Klinger, E. and Hasenauer, J. (2017), A Scheme for Adaptive Selection of Population Sizes in Approximate Bayesian Computation - Sequential Monte Carlo, in J. Feret and H. Koepll, eds, ‘Computational Methods in Systems Biology’, Vol. 10545, Springer International Publishing, pp. 128–144. Series Title: Lecture Notes in Computer Science.
- Klinger, E., Rickert, D. and Hasenauer, J. (2018), ‘pyABC: distributed, likelihood-free inference’, *Bioinformatics* (May), 1–3.
- Lynch, M. (2010), ‘Evolution of the mutation rate.’, *Trends Genet.* **26**(8), 345–352.

- Lynch, M., Sung, W., Morris, K., Coffey, N., Landry, C. R., Dopman, E. B., Dickinson, W. J., Okamoto, K., Kulkarni, S., Hartl, D. L. and Thomas, W. K. (2008), 'A genome-wide view of the spectrum of spontaneous mutations in yeast', *Genetics* **105**(27), 9272–9277.
- Mannaert, A., Downing, T., Imamura, H. and Dujardin, J. C. (2012), 'Adaptive mechanisms in pathogens: Universal aneuploidy in *Leishmania*', *Trends Parasitol.* **28**(9), 370–376.
- Möller, M., Habig, M., Freitag, M. and Stukenbrock, E. H. (2018), 'Extraordinary Genome Instability and Widespread Chromosome Rearrangements During Vegetative Growth', *Genetics* **210**(2), 517–529.
- Musacchio, A. and Salmon, E. D. (2007), 'The spindle-assembly checkpoint in space and time', *Nat. Rev. Mol. Cell Biol.* **8**(5), 379–393.
- Naylor, R. M. and van Deursen, J. M. (2016), 'Aneuploidy in Cancer and Aging', *Annu. Rev. Genet.* **50**(1), 45–66.
- Nei, M. (2013), *Mutation-Driven Evolution*, 1st edn, Oxford University Press, Oxford.
- Niwa, O., Tange, Y. and Kurabayashi, A. (2006), 'Growth arrest and chromosome instability in aneuploid yeast', *Yeast* **23**(13), 937–950.
- Otto, S. P. (2009), 'The Evolutionary Enigma of Sex', *Am. Nat.* **174**(July), S1–S14.
- Otto, S. P. and Day, T. (2007), *A biologist's guide to mathematical modeling in ecology and evolution*, Princeton University Press.
- Pavelka, N., Rancati, G., Zhu, J., Bradford, W. D., Saraf, A., Florens, L., Sanderson, B. W., Hattem, G. L. and Li, R. (2010), 'Aneuploidy confers quantitative proteome changes and phenotypic variation in budding yeast.', *Nature* **468**(7321), 321–5.
- Ram, Y., Dellus-Gur, E., Bibi, M., Karkare, K., Obolski, U., Feldman, M. W., Cooper, T. F., Berman, J. and Hadany, L. (2019), 'Predicting microbial growth in a mixed culture from growth curve data', *Proc. Natl. Acad. Sci. U. S. A.* **116**(29), 14698–14707.
- Rancati, G. and Pavelka, N. (2013), 'Karyotypic changes as drivers and catalyzers of cellular evolvability: A perspective from non-pathogenic yeasts', *Semin. Cell Dev. Biol.* **24**(4), 332–338.
- Rancati, G., Pavelka, N., Fleharty, B., Noll, A., Trimble, R., Walton, K., Perera, A., Staehling-Hampton, K., Seidel, C. W. and Li, R. (2008), 'Aneuploidy Underlies Rapid Adaptive Evolution of Yeast Cells Deprived of a Conserved Cytokinesis Motor', *Cell* **135**(5), 879–893.

- Robbins, N., Caplan, T. and Cowen, L. E. (2017), ‘Molecular Evolution of Antifungal Drug Resistance’, *Annu. Rev. Microbiol.* **71**(1), 753–775.
- Rodrigues, M. L. and Albuquerque, P. C. (2018), ‘Searching for a change: The need for increased support for public health and research on fungal diseases’, *PLoS Negl. Trop. Dis.* **12**(6), 1–5.
- Sansregret, L. and Swanton, C. (2017), ‘The Role of Aneuploidy in Cancer Evolution’, *Cold Spring Harb. Perspect. Med.* **7**(1), a028373.
- Santaguida, S. and Amon, A. (2015), ‘Short- and long-term effects of chromosome mis-segregation and aneuploidy’, *Nat. Rev. Mol. Cell Biol.* **16**(8), 473–485.
- Santaguida, S., Vasile, E., White, E. and Amon, A. (2015), ‘Aneuploidy-induced cellular stresses limit autophagic degradation’, *Genes Dev.* **29**(19), 2010–2021.
- Schvartzman, J. M., Sotillo, R. and Benezra, R. (2010), ‘Mitotic chromosomal instability and cancer: Mouse modelling of the human disease’, *Nat. Rev. Cancer* **10**(2), 102–115.
- Selmecki, A. M., Dulmage, K., Cowen, L. E., Anderson, J. B. and Berman, J. (2009), ‘Acquisition of Aneuploidy Provides Increased Fitness during the Evolution of Antifungal Drug Resistance’, *PLoS Genet.* **5**(10), e1000705.
- Selmecki, A. M., Forche, A. and Berman, J. (2010), ‘Genomic Plasticity of the Human Fungal Pathogen *Candida albicans*’, *Eukaryot. Cell* **9**(7), 991–1008.
- Selmecki, A. M., Gerami-Nejad, M., Paulson, C., Forche, A. and Berman, J. (2008), ‘An isochromosome confers drug resistance in vivo by amplification of two genes, ERG11 and TAC1’, *Mol. Microbiol.* **68**(3), 624–641.
- Sheltzer, J. M. and Amon, A. (2011), ‘The aneuploidy paradox: Costs and benefits of an incorrect karyotype’, *Trends Genet.* **27**(11), 446–453.
- Sheltzer, J. M., Ko, J. H., Replogle, J. M., Habibe Burgos, N. C., Chung, E. S., Meehl, C. M., Sayles, N. M., Passerini, V., Storchova, Z. and Amon, A. (2017), ‘Single-chromosome Gains Commonly Function as Tumor Suppressors’, *Cancer Cell* **31**(2), 240–255.
- Shor, E. and Perlin, D. S. (2015), ‘Coping with Stress and the Emergence of Multidrug Resistance in Fungi’, *PLOS Pathog.* **11**(3), e1004668.
- Sionov, E., Lee, H., Chang, Y. C. and Kwon-Chung, K. J. (2010), ‘*Cryptococcus neoformans* Overcomes Stress of Azole Drugs by Formation of Disomy in Specific Multiple Chromosomes’, *PLoS Pathog.* **6**(4), e1000848.

- Sisson, S. A., Fan, Y. and Tanaka, M. M. (2007), ‘Sequential Monte Carlo without likelihoods’, *Proc. Natl. Acad. Sci.* **104**(6), 1760–1765.
- Sunshine, A. B., Payen, C., Ong, G. T., Liachko, I., Tan, K. M. and Dunham, M. J. (2015), ‘The Fitness Consequences of Aneuploidy Are Driven by Condition-Dependent Gene Effects’, *PLOS Biol.* **13**(5), e1002155.
- Syga, S., David-Rus, D., Schälte, Y., Hatzikirou, H. and Deutsch, A. (2021), ‘Inferring the effect of interventions on COVID-19 transmission networks’, *Sci. Rep.* **11**(1), 1–11.
- Todd, R. T., Forche, A. and Selmecki, A. M. (2017), ‘Ploidy Variation in Fungi: Polyploidy, Aneuploidy, and Genome Evolution’, *Microbiol. Spectr.* **5**(4), 1–20.
- Toni, T., Welch, D., Strelkowa, N., Ipsen, A. and Stumpf, M. P. (2009), ‘Approximate Bayesian computation scheme for parameter inference and model selection in dynamical systems’, *J. R. Soc. Interface* **6**(31), 187–202.
- Torres, E. M., Dephoure, N., Panneerselvam, A., Tucker, C. M., Whittaker, C. A., Gygi, S. P., Dunham, M. J. and Amon, A. (2010), ‘Identification of aneuploidy-tolerating mutations’, *Cell* **143**(1), 71–83.
- Torres, E. M., Sokolsky, T., Tucker, C. M., Chan, L. Y., Boselli, M., Dunham, M. J. and Amon, A. (2007), ‘Effects of Aneuploidy on Cellular Physiology and Cell Division in Haploid Yeast’, *Science (80-.).* **317**(5840), 916–924.
- Tsai, H. J., Nelliat, A. R., Choudhury, M. I., Kucharavy, A., Bradford, W. D., Cook, M. E., Kim, J., Mair, D. B., Sun, S. X., Schatz, M. C. and Li, R. (2019), ‘Hypo-osmotic-like stress underlies general cellular defects of aneuploidy’, *Nature* .
- Williams, B. R., Prabhu, V. R., Hunter, K. E., Glazier, C. M., Whittaker, C. a., Housman, D. E. and Amon, A. (2008), ‘Aneuploidy Affects Proliferation and Spontaneous Immortalization in Mammalian Cells’, *Science (80-.).* **322**(5902), 703–709.
- Yona, A., Frumkin, I. and Pilpel, Y. (2015), ‘A Relay Race on the Evolutionary Adaptation Spectrum’, *Cell* **163**(3), 549–559.
- Yona, A., Manor, Y. S., Herbst, R. H., Romano, G. H., Mitchell, A., Kupiec, M., Pilpel, Y. and Dahan, O. (2012), ‘Chromosomal duplication is a transient evolutionary solution to stress.’, *Proc. Natl. Acad. Sci.* **109**(51), 21010–5.
- Zhu, J., Pavelka, N., Bradford, W. D., Rancati, G. and Li, R. (2012), ‘Karyotypic determinants of chromosome instability in aneuploid budding yeast’, *PLoS Genet.* **8**(5).

Zhu, J., Tsai, H.-J., Gordon, M. R. and Li, R. (2018), ‘Cellular Stress Associated with Aneuploidy’, *Dev. Cell* **44**(4), 420–431.

Zhu, Y. O., Sherlock, G. and Petrov, D. A. (2016), ‘Whole Genome Analysis of 132 Clinical *Saccharomyces cerevisiae* Strains Reveals Extensive Ploidy Variation’, *G3 Genes, Genomes, Genet.* **6**(8), 2421–2434.

Zhu, Y. O., Siegal, M. L., Hall, D. W. and Petrov, D. A. (2014), ‘Precise estimates of mutation rate and spectrum in yeast’, *Nature* **111**(22), E2310–E2318.

Supplementary Material

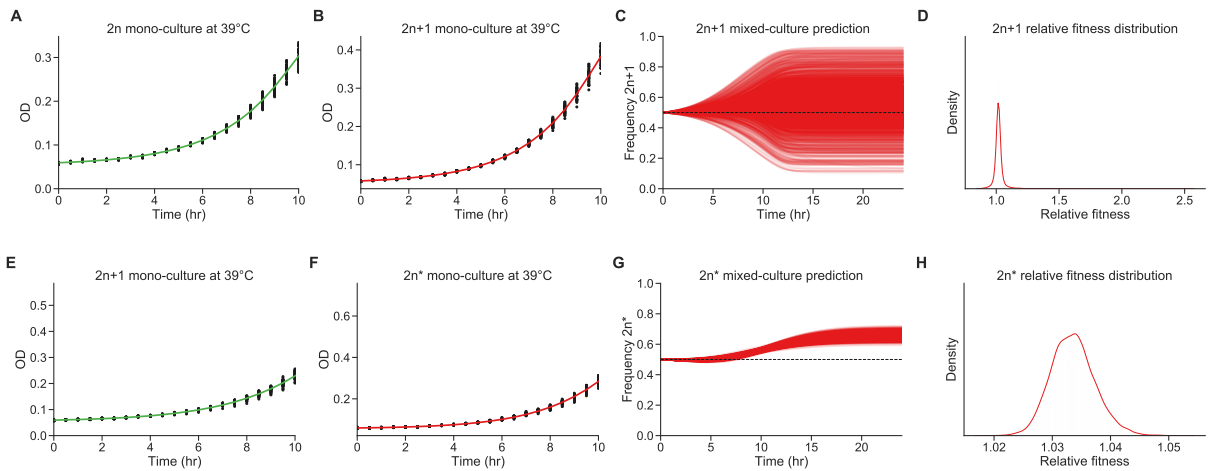


Figure S1: Fitness estimation from growth curves. (A-D) Fitness estimation from growth curves of $2n$ and $2n+1$ at 39°C . $\hat{w}_{2n+1}/w_{2n}=1.024$ (95% CI: 0.959 - 1.115). Curveball (E-H) Fitness estimation from growth curves of $2n+1$ and $2n^*$ at 39°C . $\hat{w}_{2n^*}/w_{2n+1}=1.033$ (95% CI: 1.027 - 1.041). Growth curves previously described in Yona et al. (2012, Figs. 3C, 4A, and S2). Fitness estimated from growth curves using Curveball, a method for predicting results of competition experiments from growth curve data (Ram et al., 2019, curveball.yoavram.com). See *Models and Methods, Prior distributions* for more details. (A,B;E,F) Mono-culture growth curve data (markers) and best-fit growth models (lines). (C,G) The mixed-culture prediction for the strains from A,B and E,F respectively, 6,375 generated curves. (D,H) The relative fitness distribution for $2n+1$ relative to $2n$ (panel D) and $2n^*$ relative to $2n+1$ (panel H). Figures generated by Curveball.

Table S1: WAIC values for various model specifications.

| id | Model | WAIC |
|----|---|------|
| 1 | Without aneuploidy | -35 |
| 2 | Fixed mutation rate, $\mu = 10^{-5}$, $\tau = 1$ | -16 |
| 3 | Fixed mutation rate, $\mu = 10^{-6}$, $\tau = 1$ | -38 |
| 4 | Fixed mutation rate, $\mu = 10^{-7}$, $\tau = 1$ | -53 |
| 5 | Free mutation rate, $\tau = 1$ | 295 |
| 6 | Free mutation rate, $\tau = 33/32$ | 266 |
| 7 | Free mutation rate, $\tau = 2$ | 501 |
| 8 | Free mutation rate, $\tau = 5$ | 376 |
| 9 | Free mutation rate, $\tau = 10$ | 318 |
| 10 | Free mutation rate, $\tau = 100$ | 319 |

WAIC (widely applicable information criterion; Equation 6) (Gelman et al., 2013) values for models: (1) without aneuploidy; (2-4) with aneuploidy, fixed mutation rate, and $\tau = 1$; (5-10) with aneuploidy, free mutation rate model parameter, and different τ . WAIC values are scaled as a deviance measure: lower values imply higher predictive accuracy and a difference of 2 is a popular threshold for model comparison (Kass and Raftery, 1995).

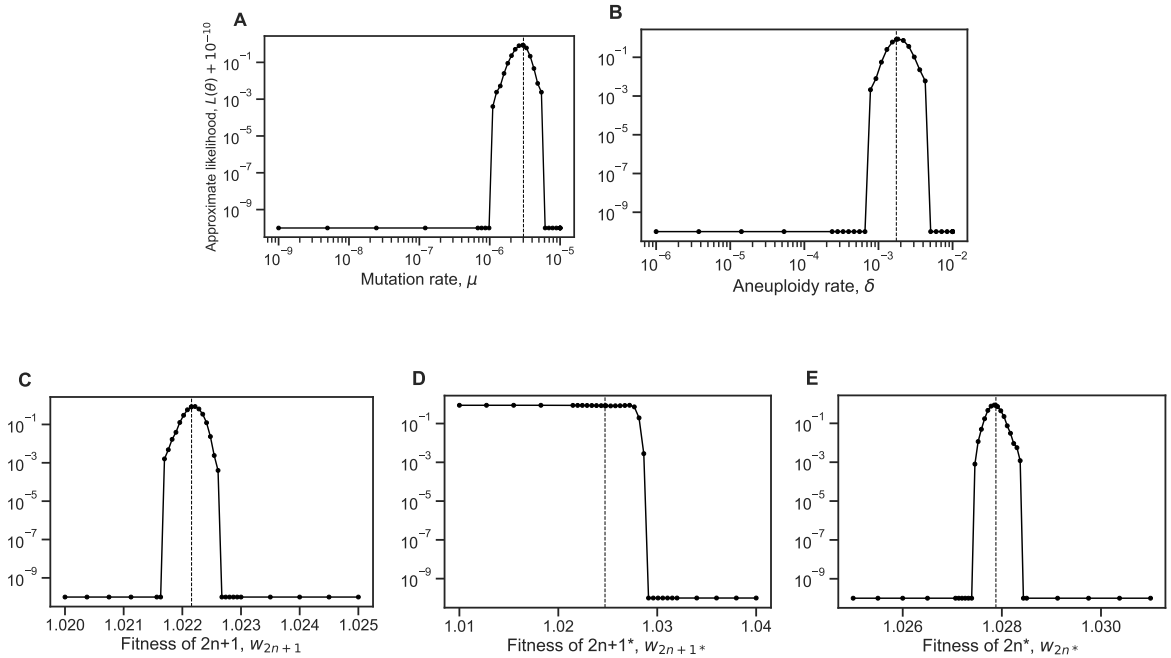


Figure S2: Likelihood profiles. Sensitivity of the model approximate likelihood, $\mathcal{L}(\theta)$, to changing a single parameter while the other parameters remain fixed at their MAP estimates. Dashed vertical line represents the MAP value. The prior distributions for the mutation rate and aneuploidy rate are $\mu \sim U(10^{-9}, 10^{-5})$ and $\delta \sim U(10^{-6}, 10^{-2})$, respectively.

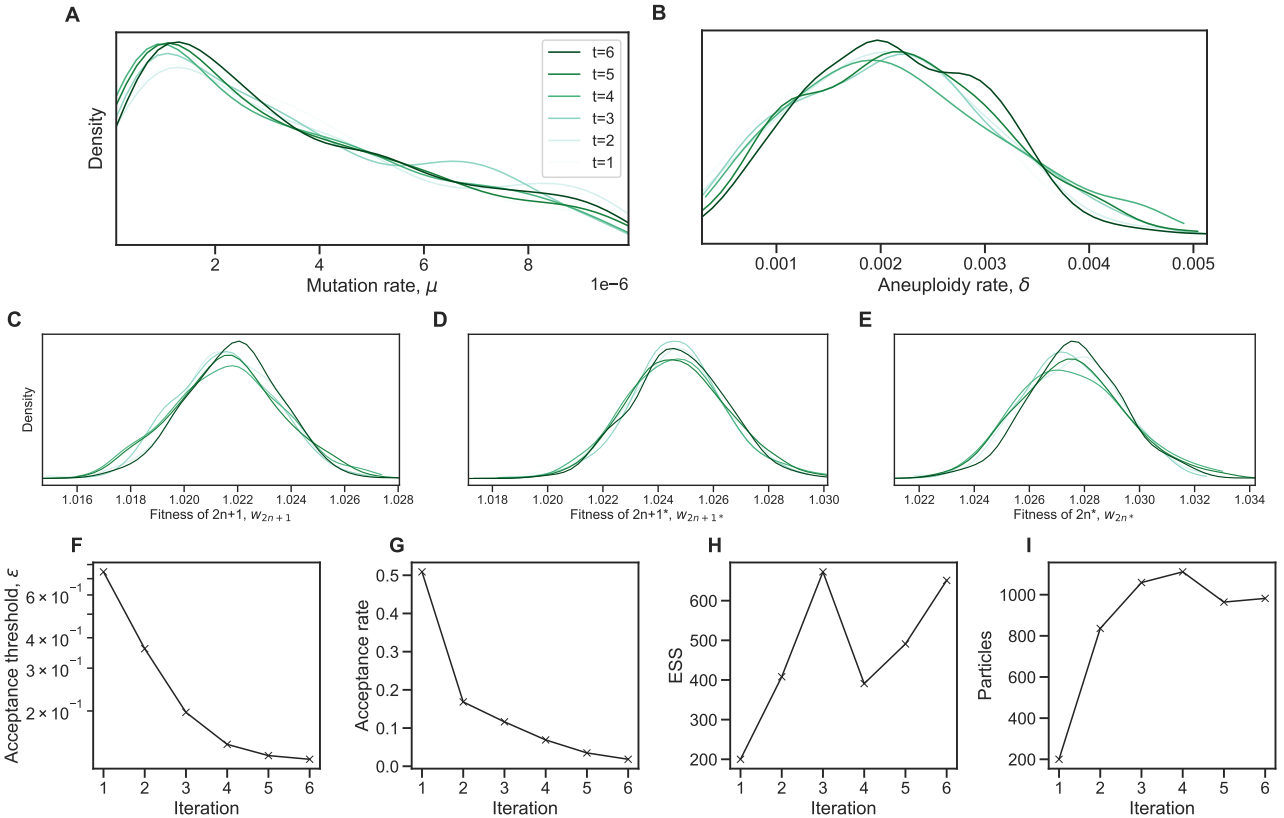


Figure S3: Inference convergence. The ABC-SMC algorithm was used to infer the model parameters. **(A-E)** The approximate posterior distributions of model parameters at each iteration of the ABC-SMC algorithm demonstrates convergence, as the posterior did not significantly change after the first iteration, $t = 1$. **(F-I)** ABC-SMC measures of convergence. After iteration number 6, the acceptance threshold was $\epsilon = 0.13$, the acceptance rate was 0.018, the number of particles was 982, and the effective sample size ESS=651.

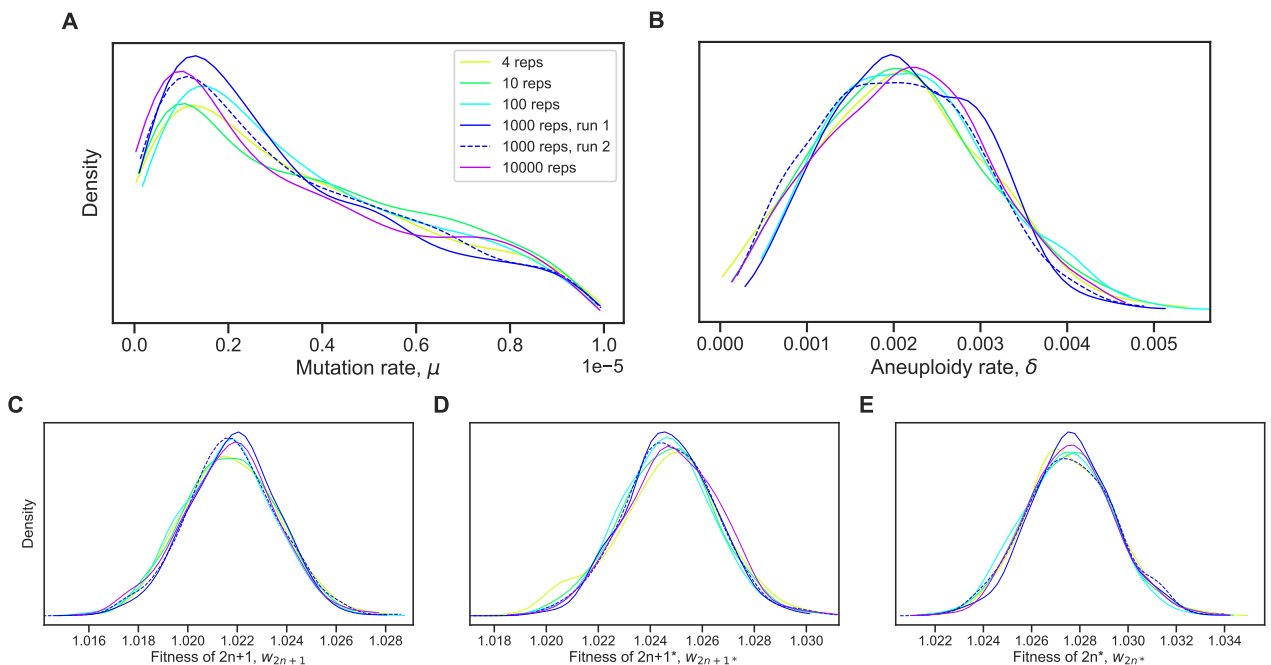


Figure S4: Posterior distribution validation. The posterior distribution of model parameters is roughly the same regardless of the number of simulations (4-10,000 replicates) used to approximate the likelihood (Equation (4)).

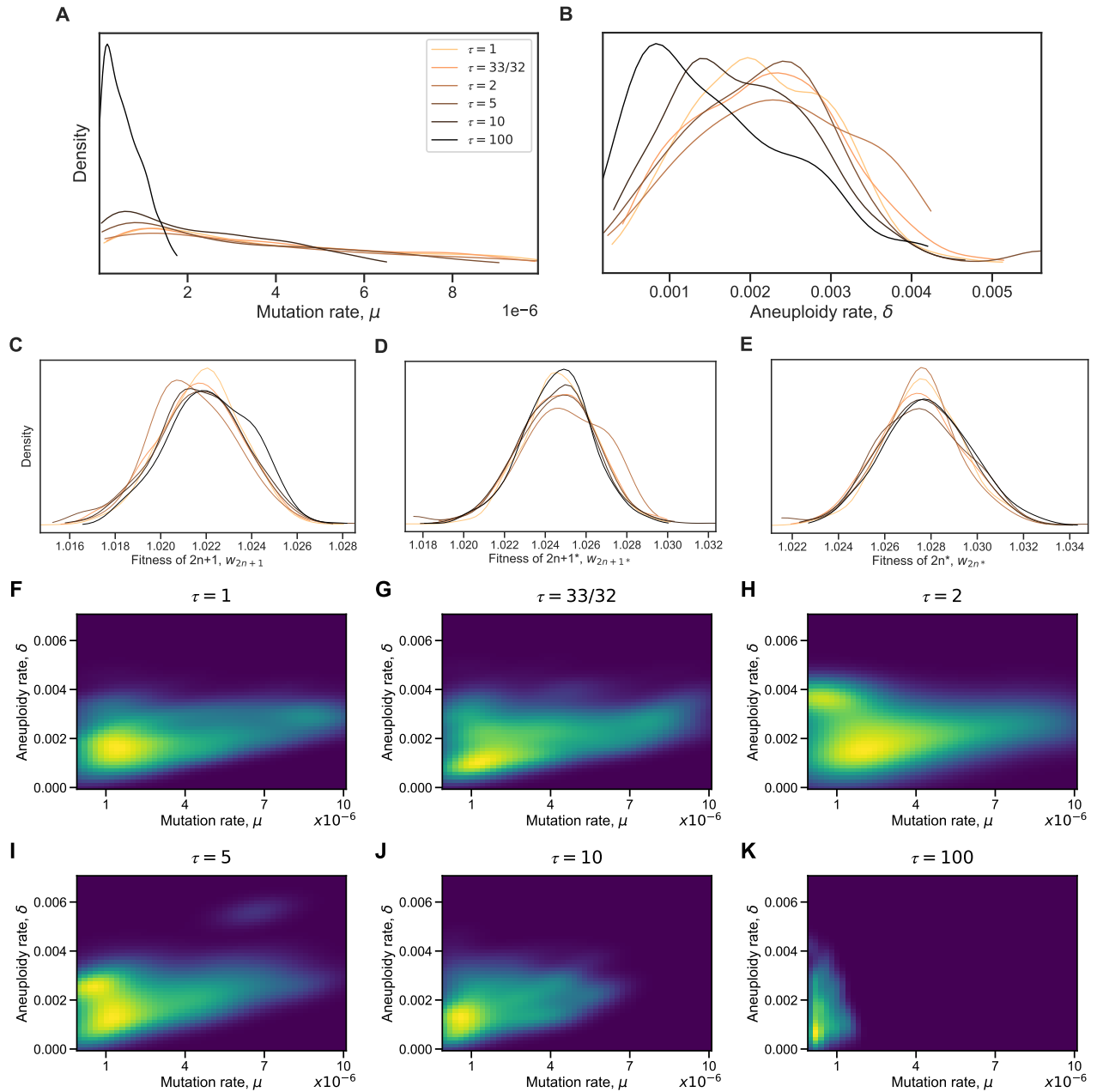


Figure S5: Model with elevated mutation rate in aneuploid cells. (A-E) The inferred posterior distributions for models with different values of τ , the fold-increase in mutation rate in aneuploid cells ($2n+1$ and $2n+1^*$). When the increase in mutation rate is high, $\tau = 10$ and $\tau = 100$, the inferred mutation (A) and aneuploidy (B) rate tends to be lower. (F-K) The inferred joint posterior distribution of mutation rate (μ) and aneuploidy rate (δ) with different τ values (dark purple and bright yellow for low and high density, respectively).

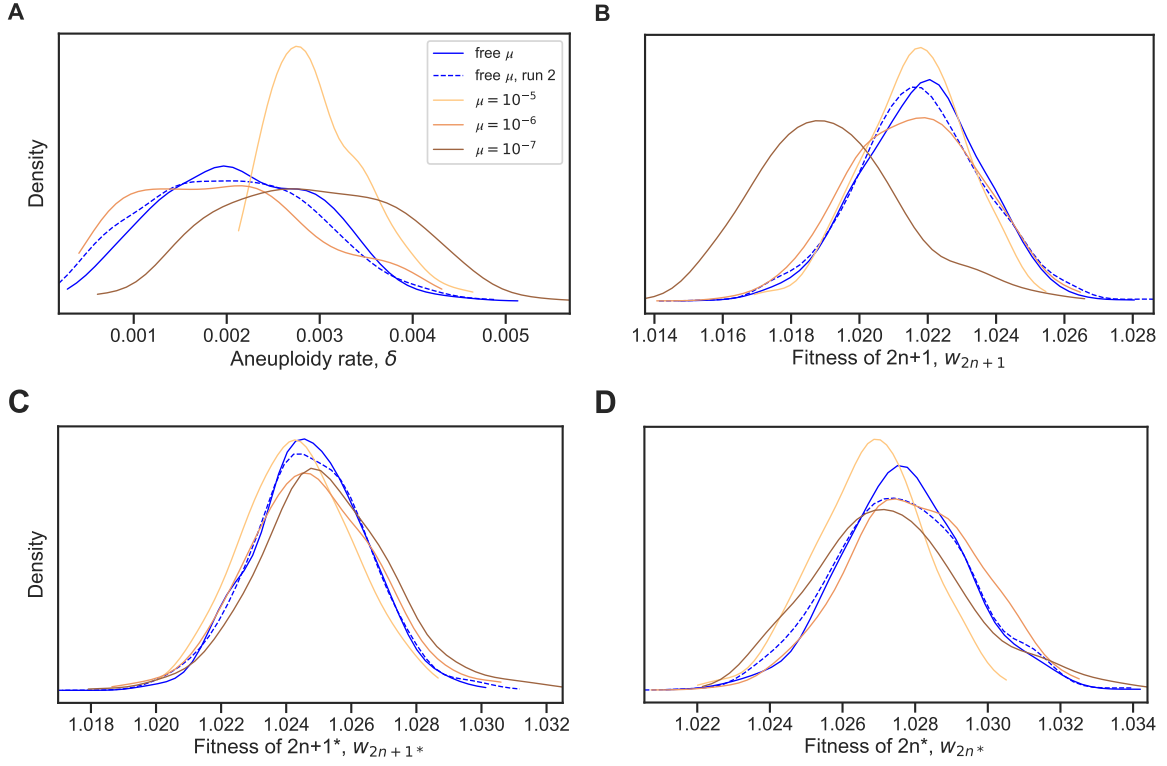


Figure S6: Model with fixed mutation rate. (A-D) The inferred posterior distributions for models with free and fixed mutation rate, μ . The MAP (maximum a posteriori) and 50% HDI (highest density interval) for each model are following: **free μ :** $\delta = 2.749 \cdot 10^{-3}$ [$1.476 \cdot 10^{-3} - 2.822 \cdot 10^{-3}$], $w_{2n+1} = 1.022$ [1.021 – 1.023], $w_{2n+1}^* = 1.025$ [1.023 – 1.026], $w_{2n}^* = 1.027$ [1.026 – 1.029]; **free μ , run 2:** $\delta = 1.938 \cdot 10^{-3}$ [$1.338 \cdot 10^{-3} - 2.748 \cdot 10^{-3}$], $w_{2n+1} = 1.022$ [1.02 – 1.023], $w_{2n+1}^* = 1.025$ [1.023 – 1.026], $w_{2n}^* = 1.027$ [1.026 – 1.029]; **$\mu = 10^{-5}$:** $\delta = 3.089 \cdot 10^{-3}$ [$2.412 \cdot 10^{-3} - 3.169 \cdot 10^{-3}$], $w_{2n+1} = 1.022$ [1.021 – 1.023], $w_{2n+1}^* = 1.024$ [1.023 – 1.026], $w_{2n}^* = 1.027$ [1.026 – 1.028]; **$\mu = 10^{-6}$:** $\delta = 1.413 \cdot 10^{-3}$ [$1.04 \cdot 10^{-3} - 2.529 \cdot 10^{-3}$], $w_{2n+1} = 1.021$ [1.02 – 1.023], $w_{2n+1}^* = 1.024$ [1.023 – 1.026], $w_{2n}^* = 1.028$ [1.026 – 1.029]; **$\mu = 10^{-7}$:** $\delta = 3.4 \cdot 10^{-3}$ [$2.043 \cdot 10^{-3} - 3.578 \cdot 10^{-3}$], $w_{2n+1} = 1.019$ [1.017 – 1.02], $w_{2n+1}^* = 1.026$ [1.024 – 1.027], $w_{2n}^* = 1.027$ [1.026 – 1.029].